JOURNAL OF SOLID STATE CHEMISTRY 112, 148–156 (1994)

Spin State and Variation of the Spin Orientation of Co(III) in the 112-Type Phase $YBa(Co_{2-x}Cu_x)O_5$

L. Barbey, N. Nguyen, V. Caignaert, F. Studer, and B. Raveau

Laboratoire CRISMAT-ISMRA, Université de Caen, Boulevard du Maréchal Juin, 14050 Caen Cedex, France

Received July 2, 1993; in revised form November 1, 1993; accepted November 4, 1993

The copper and cobalt valence states in the 112-phase $YBa(Co_{2-x}Cu_x)O_5$ have been determined from a XANES analysis: copper is mainly in the Cu(II) state whereas cobalt appears in a mixed valent state Co(II)/Co(III) in agreement with the oxygen stoichiometry. The magnetic behavior of cobalt and copper in the structure of these compounds has been determined by magnetic susceptibility measurements and by powder neutron diffraction. The evolution of inverse molar susceptibility versus temperature shows that these phases are antiferromagnetic with T_N ranging from 395 to 515 K. At low temperature ($T < T_N$), one observes a second magnetic transition for $0.75 < x < 1.0$ compositions. The temperature $T2$ corresponding to this transition increases when x decreases. The nuclear and magnetic structures of three compositions, $x = 0.4$, 0.8, and 0.9, have been investigated by neutron diffraction at 1.4 K. At this temperature, the nuclear structure of these phases has the space group $P4/mmm$ and lattice parameters $a_0 = a_p$ and $c_0 = 2a_p$. The magnetic cell is related to the nuclear cell by the relationships: $a = a_0\sqrt{2}$, $c = c_0$ for $x = 0.4$ and $a = a_0\sqrt{2}$, $c = 2c_0$ for $x = 0.8$ and 0.9. For the $x = 0.4$ compound, the magnetic moments lie in the ab plane; on the other hand, the spins exhibit another component along c for $x = 0.8$ and 0.9 phases. The study of the magnetic structure of the $x = 0.8$ oxide versus temperature shows that their spins switch along the c axis as the temperature approaches $T2$. The values of the magnetic moment determined in this study for these phases agree with the $t_{2g}^5e_g^1$ configuration of the Co(III) ion.

INTRODUCTION

The relationship between superconductivity and magnetism in high T_c cuprates is not yet completely understood. For this reason, a tremendous number of magnetic studies have been performed on layered cuprates, and especially on the "123"-phase $YBa_2Cu_3O_{7-\delta}$ in which copper is partly replaced by a magnetic ion, namely iron and cobalt. The study of the latter phase is complicated by the possible variation of the oxygen stoichiometry with the substitution rate. In this respect the layered 112-cuprate $YBaFeCuO_5$ (1) is an interesting material, due to the simplicity of its oxygen-deficient perovskite structure which is only built up of corner-sharing CuO_5 and FeO_5 pyramids; moreover the oxygen stoichiometry of this phase is much less sensitive to the oxygen pressure and tends to keep the "O_5" composition for the samples quenched in air.

The magnetic study of cobalt is also interesting, compared to iron, owing to its great ability to take intermediate-spin configuration. In most of the Fe(III) oxides, Fe(III) indeed exhibits an in-plane high-spin configuration. This is not the case for Co(III), whose field energy close to the exchange energy allows transitions (2, 3) by varying the temperature between the high-spin state $t_{2g}^4e_g^2$ ($S = 2$), the low-spin state t_{2g}^6 ($S = 0$), and the intermediate-spin state $t_{2g}^5e_g^1$ ($S = 1$). Several examples of low-spin to high-spin transition have been evidenced in cobalt oxides with the K_2NiF_4 structure such as $A_{0.5}La_{1.5}Mg_{0.5}Co_{0.5}O_4$ (A = Ba, Sr, Ca) (3) and La_4LiCoO_8 (4) and with the perovskite structure such as $LnCoO_3$ (5, 6). In the same way, an intermediate-spin state configuration in the K_2NiF_4-type oxide $La_2Li_{0.5}Cu_{0.4}Co_{0.1}O_4$ (7) and a low- to intermediate-spin transition for $Sr_4(Ta, Nb)CoO_8$ (4) were evidenced. Nevertheless in all these oxides, cobalt is characterized by a squeezed or elongated octahedral coordination, so that its behavior cannot be directly transposed to the pyramidal coordination observed for many cuprates. Only one 2H-related hexagonal perovskite, $Sr_2Co_2O_5$ (8), with a pyramidal coordination of cobalt has been studied up to now. For the latter, the authors thought that cobalt with intermediate spin should be located on two sites of lower coordination: pyramidal site and square planar site.

In order to understand the complex magnetic behavior of cobalt in such structures, the 112-phase $YBa(Co_{2-x}Cu_x)O_5$ was recently synthesized (9) with a homogeneity range significantly larger than that obtained by Lin *et al.* (10). The present paper deals with the study of the magnetic structure and properties of these oxides; it establishes relationships between the spin orientations of Co(III) and the distortion of the $Co(Cu)O_5$ pyramid.

EXPERIMENTAL

Polycrystalline samples of the pure phase $YBa(Co_{2-x}Cu_x)O_{5\pm\delta}$ were prepared by solid-state reaction of Y_2O_3,

0022-4596/94 $6.00

$BaCO_3$, and Co_3O_4 in molar ratios according to the nominal composition. The mixtures were calcined in air at 900°C to ensure decarbonation and then heated at 1000°C for 24 hr. They were quenched to room temperature in air. X-ray powder diffractograms were recorded from a Philips goniometer working with Cu$K\alpha$ radiation. The deviation from oxygen stoichiometry δ was chemically checked by iodometric titration and by thermogravimetric analysis by heating the powder from 298 to 1240 K in a mixed atmosphere of 10% H_2 in Ar. The neutron diffraction patterns were registered at different temperatures using the multicounter diffractometers G41 and 3T2 installed at Saclay. A neutron wavelength of 2.426 and 1.2268 Å was used to collect data by step scanning over an angular range of $10° \leq 2\theta \leq 90°$ and of $5 \leq 2\theta \leq 120°$ for G41 and 3T2 diffractometers, respectively. The refinement of the crystal structure was performed with the profile refinement computer program FULLPROF (11). Magnetic susceptibility measurements were carried out from 77 to 850 K using the Faraday method.

The XAS spectra at the Co K-edge were recorded at room temperature on powder samples in transmission mode. The experiments were performed at LURE (ORSAY) using the synchrotron radiation from the DCI storage ring operated at 1.85 GeV with a nominal current of 250 mA. X-rays were monochromatized by a Si (331) channel cut and the incident and transmitted intensities were measured using two ionization chambers. The energy resolution was estimated to be better than 0.8 eV at the Co K-edge, whereas the reproductibility of the energy position of the spectral features is close to 0.3 eV.

The normalization procedure used throughout this work was a standard one: after substraction of the same background out of the XANES and EXAFS spectra, recorded under the same experimental conditions, a point located at an energy of 800 eV from the edge, where no more EXAFS oscillations were still observable, was set to unity.

XAS spectra at the L_3-edge of copper were recorded at room temperature on powder samples by a fluorescence yield method. The experiments were performed at LURE (Orsay) using the synchrotron radiation from the super-ACO ring operated at 800 MeV with a typical current of 250 mA. Samples were ground and sieved homogeneously on a sticky band supported by an aluminum sample holder. Electrical contacts were realized by silver paste dots. The X rays were monochromatized by two beryl crystals $(10\bar{1}0)$ and focused by a TiN-coated parabolic mirror to give into a 0.5-mm-diameter spot. The fluorescence yield was detected by a seven-Ge diode detector with an axis at 45° from the beam line. The energy scale was then positioned with respect to the $|3d^9\rangle$ peak of CuO at 931.2 eV. The experimental energy resolution was estimated to be better than 0.3 eV, whereas the reproducibility of the energy position of the spectral features is close to 0.05 eV. The width of the core hole has been measured to be 0.3 eV at the L_3-edge. The usual thickness of the probed upper layer of the samples is about 2000 Å in the fluorescence yield method. The top of the $|3d^9\rangle$ transitions for all the compounds has been set to a common value chosen arbitrarily.

RESULTS AND DISCUSSION

For different air-quenched samples of pure-phase YBa$(Co_{2-x}Cu_x)O_5$ with $0.3 \leq x \leq 1$, the chemical analysis combined with microthermogravimetric analysis allowed the oxygen content very close to "O_5" to be established for whatever x. As will be shown below, this oxygen stoichiometry was confirmed by the neutron diffraction study of several of these oxides.

XANES

XANES spectroscopy has been proven to be a valuable tool for the determination of the electronic structure above the Fermi level (first empty levels) and of the valence state of the elements in solids (12–19). In order to establish the various oxidation states of copper and cobalt in the materials studied, a XANES investigation has been performed for several samples, $x = 0.4$, 0.8, and 0.9.

Copper Valence

In oxides, like HTC superconductors, copper can present simultaneously the three known valence states Cu(I), Cu(II), and Cu(III). To demonstrate this point in the YBa$(Co_{2-x}Cu_x)O_5$ solid solution, we have recorded the Cu K- and L_3-edges of some reference copper oxides, Cu_2O for Cu(I) and La_2CuO_4 and Nd_2CuO_4 for Cu(II). Both the latter compounds exhibit somewhat different copper coordination with an elongated oxygen octahedron for La_2CuO_4 and a square plane for Nd_2CuO_4, leading for the latter to a more pronounced z-polarized contribution in the copper K-edge spectrum. But, in both cases, the Cu$3d_{x^2-y^2}$ orbital is the only one which contains the covalent holes. A detailed analysis of copper electronic configurations in various valence states has been published in many papers (20–27) and can be summarized in the following way: Cu(I) in the $3d^{10}$, Cu(II) in the $\alpha|3d^9> + \beta|3d^{10}\underline{L}>$ with $\beta > \alpha$, and Cu(III) in the $|3d^9\underline{L}\rangle$ configurations, respectively. Both the latter configurations are due to a charge transfer mechanism predominant in copper oxides.

The Cu(I) valence. At the Cu K-edge, the Cu_2O spectrum shows a peak at 1.3 eV (Fig. 1a) due to the $1s \rightarrow 4p$ transition in the $3d^{10}$ configuration and characteristic of Cu(I). Such a peak is totally absent from the La_2CuO_4 spectrum and from the spectra of $YBa(Co_{1.1}Cu_{0.9})O_5$ and

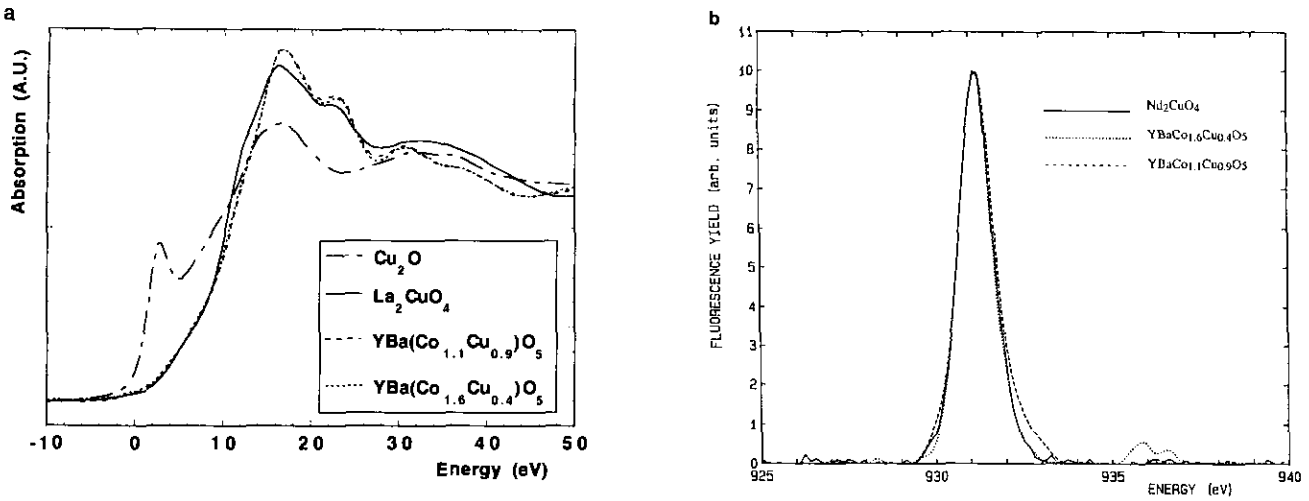

FIG. 1. (a) The copper K-edges of some reference oxides (Cu_2O for Cu(I), La_2CuO_4 for Cu(II) and of two compositions in the $YBa(Co_{1-x}Cu_x)O_5$ solid solution. (b) The copper L_3-edges of a reference oxide (Nd_2CuO_4 for Cu(II) and two compositions in the $YBa(Co_{1-x}Cu_x)O_5$ solid solution.

$YBa(Co_{1.6}Cu_{0.4})O_5$. Thus one can conclude to the absence of Cu(I) in the $YBa(Co_{2-x}Cu_x)O_5$ solid solution with a precision better than 5%.

The Cu(III) valence. At the Cu L_3-edge, the reference compound for Cu(II), Nd_2CuO_4, shows only one symmetric peak (Fig. 1b) due to the $|2p^63d^9> \rightarrow |c2p^53d^{10}\rangle$ transition. The Cu L_3-edge spectrum of the compound La_2CuO_4 looks identical to that of Nd_2CuO_4. As it has been shown by previous works (12, 15–18), the "Cu(III)" valence appears as a shoulder on the high-energy side of the main peak (≈933 eV) due to the $|2p^63d^9\underline{L}> \rightarrow |c2p^53d^{10}\underline{L}\rangle$ transition. The Cu L_3-edge of the Cu(III) compound, $La_2Li_{0.5}Cu_{0.5}O_4$, has been published previously (27) and has been shown to exhibit only the $|3d^9\underline{L}\rangle$ peak at 933.2 eV. Such a shoulder appears only as a small dissymmetry on the high-energy side of the main peak for the highest copper concentration ($x = 0.8$ and 0.9) of the $YBa(Co_{2-x}Cu_x)O_5$ solid solution: a simulation with two Lorentzians gives 7% Cu(III) out of total copper. In the case of low copper concentration ($x = 0.4$), no Cu(III) was detected at least within the precision of the determination (5%).

It is concluded that copper exhibits mainly the Cu(II) valence state in the whole homogeneity domain of the $YBa(Co_{2-x}Cu_x)O_5$ solid solution.

Cobalt Valence

In oxides, cobalt can be found mainly in the Co(II) and Co(III) valence states. Co(II) appears most of the time as a high-spin $3d^7$ cation. As with copper, the real electronic configuration of Co(II) can be written $\alpha|3d^7> + \beta|3d^8\underline{L}\rangle$, taking into account the Co–O covalence through the charge transfer model but here $\beta < \alpha$ (28). Co(II) has been observed in octahedral, tetrahedral, and square plane environments whereas Co(III) has been mainly observed in octahedral and tetrahedral environments. We have chosen cobalt carbonate $CoCO_3$, isotype of calcite, as a reference for Co(II) in a slightly distorted octahedron ($d_{Co-O} \approx 2.02$ Å), the spinel $CoAl_2O_4$ as a reference for Co(II) in tetrahedra ($d_{Co-O} \approx 1.95$ Å) (29), and $LaCoO_3$ for Co(III) in octahedra ($d_{Co-O} \approx 1.92$ Å) (30).

Reference compounds. At the cobalt K-edge, $CoCO_3$ exhibits a very simple spectrum (Fig. 2a) with a main white line at 15.5 eV corresponding to the $|1s^23d^74p^0> \rightarrow |1s^13d^74p^1\rangle$ electronic transition. A very weak prepeak can be observed around 0 eV, likely due to some quadrupolar effect since the $1s \rightarrow 3d$ transition is dipole forbidden.

Conversely the $CoAl_2O_4$ edge is much more complex and exhibits at least five contributions noted A, B, C, D and E in Fig. 2a. Prepeak A is rather intense, in agreement with the hybridization of Co $3d$ and $4s$ atomic orbitals via the O $2p$ orbitals which is possible in the noncentrosymmetric crystal field of the tetrahedra. For the structure of the main edge (peaks B, C, D, and E), one must take into account the distortion of the tetrahedra which splits the $4p$ orbitals in a low-energy $4p_z$ nonbonding and high-energy $4p_{x,y}$ antibonding molecular orbitals. By analogy with the copper case and using the electronic configuration of Co(II) expressed above, peaks B and C could be understood to be due to the $1s \rightarrow 4p_z$ transition in the $3d^8\underline{L}>$ and $|3d^7\rangle$ configurations, respectively, the former being stabilized and reinforced by a smaller interaction with the core hole than the latter. The same situation occurs for the $1s \rightarrow 4p_{x,y}$ transition (peaks D and E) with a weak $|3d^7\rangle$ configuration probably partially masked by the intensity of peak D. XANES simulations should be performed to test this hypothesis.

Compound $LaCoO_3$ has been synthesized in a normal pressure oxygen flux at 900°C. By thermogravimetric

TABLE 1

Equivalent Edge Energies (Eq) and Calculated Mean Cobalt Formal Charges (q_{Co}) Compared to Those Deduced from the Normal Oxygen Stoichiometry for the $YBa(Co_{2-x}Cu_x)O_5$ Solid Solution

Compounds	Eq (eV)	q_{Co}	q_{Co} for a normal oxygen stoichiometry
$CoCO_3$	6.8	2.0	2.0
$CoAl_2O_4$	7.4	2.0	2.0
Co_3O_4	9.5	2.7	2.66
$LaCoO_3$	10.5	3.0	3.0
$YBa(Co_{1.6}Cu_{0.4})O_5$	8.7	2.5	2.62
$YBa(Co_{1.2}Cu_{0.8})O_5$	9.2	2.65	2.8
$YBa(Co_{1.1}Cu_{0.9})O_5$	9.6	2.75	2.9

analysis, the oxygen stoichiometry has been shown to be $LaCoO_{3\pm0.03}$ and the cobalt valence is thus close to III. The $LaCoO_3$ spectrum (Fig. 2a) exhibits only a white line at 18 eV corresponding to the $|1s^2 3d^7 4p^0> \rightarrow |1s^1 3d^7 4p^1\rangle$ electronic transition. Prepeak A is more intense than that in $CoCO_3$, which suggests that a slight distortion of the CoO_6 octahedra occurs: it exhibits a two peak structure which can be correlated to the Co $3d(t_{2g})$ and $3d(e_g)$ orbitals and shows that Co(III) cannot be in the low-spin state in this compound.

A large energy shift can be observed between the $CoCO_3$ and the $LaCoO_3$ spectra in agreement with the respective cobalt valences. A quantitative analysis of the edge positions can be realized using a method proposed first by Alp *et al.* (13) which replaces the real spectrum by an equivalent square-shaped edge whose energy position can be estimated. Such an analysis has been performed on the three reference edges and the results (Table 1) show that a large energy shift exists between the Co(II) and the Co(III) references ($\Delta E \approx 3.4$ eV) and that the edge energies of both references for Co(II) are close together around 7 eV.

In order to check the validity of Alp's method, the edge of the mixed-valence spinel Co_3O_4 has been recorded (Fig. 2a). In this compound, one-third of the cobalt is Co(II) in tetrahedral environment and the last two-thirds are Co(III) in octahedral coordination, which leads to a mean cobalt formal charge of 2.66. Indeed the spectrum of Co_3O_4 corresponds to a mixture of tetrahedral Co(II) (peaks B and C like in $CoAl_2O_4$) and octahedral Co(III). A mean cobalt valence can be deduced assuming a linear relationship between valence state, from Co(II) to Co(III), and edge position. The equivalent edge position (Table 1) for Co_3O_4 leads to 2.7 for the mean cobalt formal charge in good agreement with the expected charge.

The $YBa(Co_{2-x}Cu_x)O_5$ solid solution. The spectra for $x = 0.4$, 0.8, and 0.9 are shown on Fig. 2b with the reference compounds. For the three compositions, the large intensity of the prepeaks corresponds to a strong noncentrosymmetry of the local polyhedra around cobalt, in agreement with previous observations and the presence of the metallic cation (Co, Cu) in a distorted pyramid. The shift of prepeak A toward high energy with respect to the $CoAl_2O_4$ prepeak can be correlated to an increase of the mean cobalt valence.

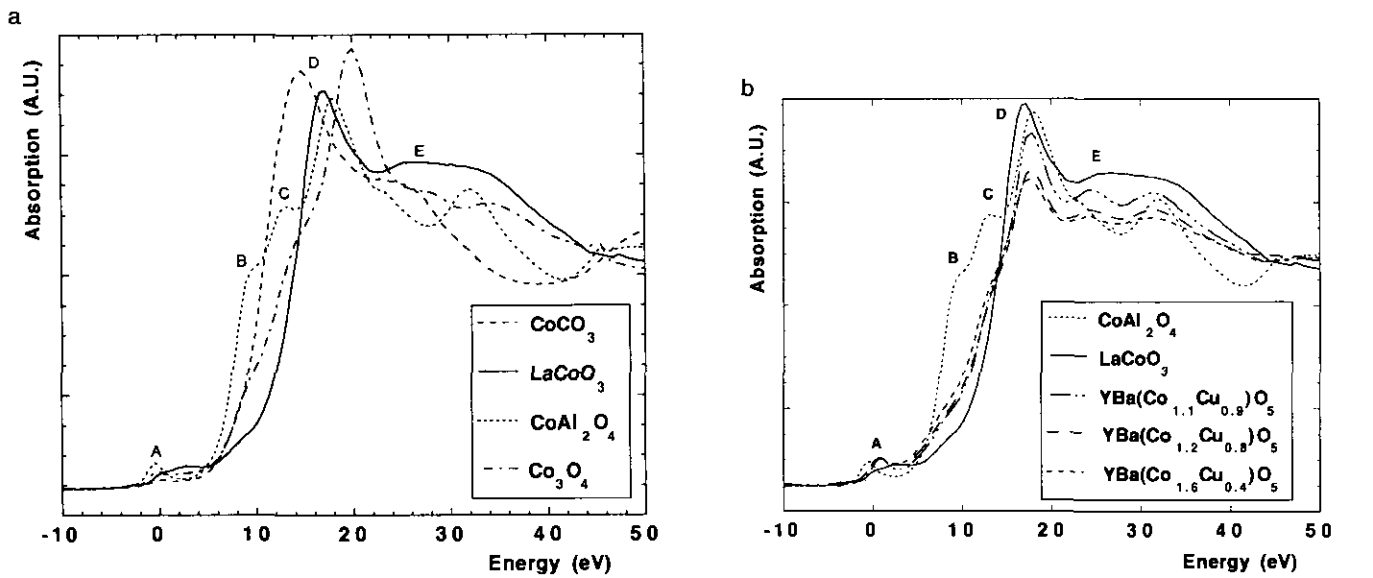

FIG. 2. (a) The cobalt K-edges of the reference cobalt oxides: $CoCO_3$ for Co(II) in octahedron, $CoAl_2O_4$ for Co(II) in tetrahedron, $LaCoO_3$ for Co(III) in octahedron, and the mixed valent spinel Co_3O_4. (b) The cobalt K-edges of some reference cobalt oxides ($CoAl_2O_4$, $LaCoO_3$) and of three compositions in the $YBa(Co_{1-x}Cu_x)O_5$ solid solution.

The equivalent edge energies calculated following Alp's method confirms this point (Table 1). Although systematically smaller (by 15%) than the mean cobalt charge deduced from an exact O_5 stoichiometry, the variation of the cobalt formal charge with x follows the expected change and confirms the mixed valence Co(II)/Co(III) in the $YBa(Co_{2-x}Cu_x)O_5$ solid solution.

From this first investigation it appears clearly that copper is close to the divalent state, whereas cobalt has mixed valence according to the formulation $YBa(Co^{(II)}_{1-x}Co^{(III)}Cu^{(II)}_x)O_5$.

NEUTRON DIFFRACTION AND MAGNETIC STUDY

The susceptibility measurements performed for different x values (0.3, 0.4, 0.6, 0.75, 0.8, 0.85, 0.9, and 1) allow two kinds of magnetic behaviors to be evidenced as shown in Fig. 3. For a first domain (I) corresponding to $0.3 \leq x \leq 0.75$, the curves $\chi_M^{-1} = f(T)$ exhibit a minimum characteristic of a classical antiferromagnetic–paramagnetic transition (Fig. 3). The Neel temperature, labeled $T1$, which corresponds to this minimum, ranges from 395 to 407 K (Table 2). The second domain (II), with $0.75 < x < 1$, exhibits two minima, i.e., two transition temperatures labeled $T2$ and $T3$. Note that the $T2$ temperature decreases as x increases, whereas $T3$ that corresponds to the antiferromagnetic–paramagnetic transition increases.

In order to understand these different behaviors, a neutron diffraction study was carried out for these compounds. In a first step, the nuclear structure was studied for two compositions: $x = 0.4$ (domain I) and $x = 0.8$ (domain II) at 300 and 80 K, respectively, with the diffraction data collected on the 3T2 diffractometer. For the two samples, a large number of reflections were indexed in the expected tetragonal cell with $a_0 = a_p$ and $c_0 = 2a_p$.

TABLE 2
$YBa(Co_{2-x}Cu_x)O_5$: Evolution of Transition Temperatures

x Composition	$T1$ (±5 K)	$T2$ (±5 K)	$T3$ (±5 K)
0.3	395	—	—
0.4	408	—	—
0.5	422	—	—
0.6	419	—	—
0.7	410	—	—
0.75	407	407	—
0.8	—	310	450
0.85	—	210	479
0.9	—	180	480
1	—	—	515

The preliminary refinements performed in the nuclear cell with the space group $P4/mmm$, starting from the powder X-ray data previously obtained (9), allowed the R_I factors to be lowered to about 0.05, whatever x (Figs. 4a and 4b).

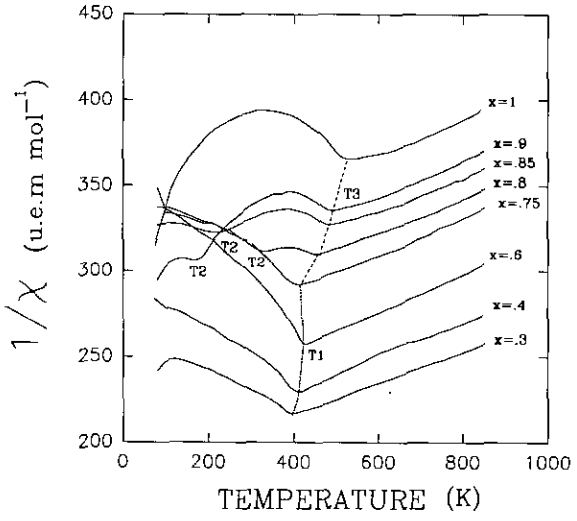

FIG. 3. Reciprocal molar magnetic susceptibility vs temperature of $YBa(Co_{2-x}Cu_x)O_5$ compounds.

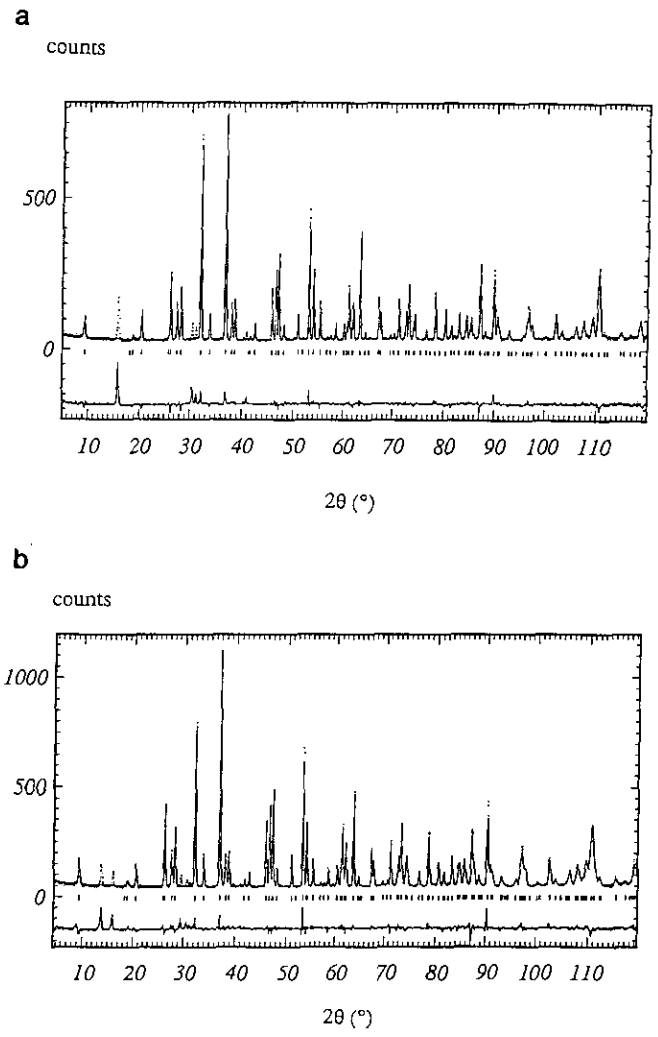

FIG. 4. Observed, calculated, and difference plots for compound (a) $YBa(Co_{1.6}Cu_{0.4})O_5$ at 300 K and compound (b) $YBa(Co_{1.2}Cu_{0.8})O_5$ at 80 K.

In the second step, a neutron diffraction study was carried out for three compositions, $x = 0.4$ (domain I) and $x = 0.8$ and 0.9 (domain II) at 1.4 K, i.e., in the antiferromagnetic state, with the diffraction data recorded with the G41 diffractometer. Several strong extra reflections could not be indexed in the tetragonal cell a_0, c_0; the variation of their intensity with temperature suggested a magnetic ordering on cobalt and copper ions in agreement with the susceptibility measurements. Thus, the patterns were finally indexed in a tetragonal cell with $a = a_0\sqrt{2}$ and $c = c_0$ for $x = 0.4$ and $a = a_0\sqrt{2}$ and $c = 2c_0$ for $x = 0.8$ and 0.9. The preliminary refinements performed in the nuclear cell a_0, c_0 with the space group $P4/mmm$ allowed the R_N factors to be lowered to values ranging from 0.037 and 0.058 (Table 3). The refinements were then performed in the magnetic cell using the same centrosymmetric space group. Several models of the antiferromagnetic interactions between different Co and Cu sites were considered, taking into account the doubling of the c parameter in the $x = 0.8$ and 0.9 compounds.

The R_M factors were finally lowered to $R_M = 0.079$ for $x = 0.4$ and $R_M = 0.139$ for $x = 0.8$ and 0.9 (Table 3), for the atomic parameters listed in Table 3. The calculated and observed patterns of two of these samples, for $x = 0.4$ (Fig. 5a) and $x = 0.9$ (Fig. 5b), show the validity of our refinements.

Consideration of the nuclear structure of these oxides confirms that the oxygen content is fixed at "O_5" (Table 4). One observes that the equatorial Co(Cu)–O_1 distances of the (Co, Cu)O_5 pyramids do not vary significantly whatever x and remain fixed at about 1.96 Å. On the contrary, the apical Co(Cu)–O_2 distance of the pyramids increases as x increases from 0.4 to 1 (Table 5), i.e., as the copper content increases, in agreement with the Jahn–Teller effect of Cu(II). Note that the pyramids of domain II are much more elongated than those of domain I. On XANES spectra (Fig. 2b), one can see that the intensities of peaks B and C increase when x decreases, in agreement with the shortening of the apical Cu–O distances deduced from neutron diffraction (Table 5) which increases the Cu $3d$ and O $2p$ overlap along the c axis. In the same way the decrease of peaks D and E when x decreases corresponds to the increase of the Cu–O distances in the x, y plane.

This study shows also that at low temperature ($T = 1.4$ K) the magnetic moments of cobalt and copper ions,

TABLE 3
Collection of R Factors and Magnetic Arroments at 1.4 K in $YBa(Co_{2-x}Cu_x)O_5$ Compounds ($x = 0.4, 0.8, 0.9$)

x Composition	R_N (%)	R_M (%)	μ_x (μ_B)	μ_z (μ_B)	$\langle\mu\rangle$ (μ_B)
0.9	3.66	13.90	1.55(6)	2.99(4)	3.37(4)
0.8	3.69	13.90	2.69(3)	2.51(3)	3.68(4)
0.4	5.81	7.89	4.59(4)	—	4.59(4)

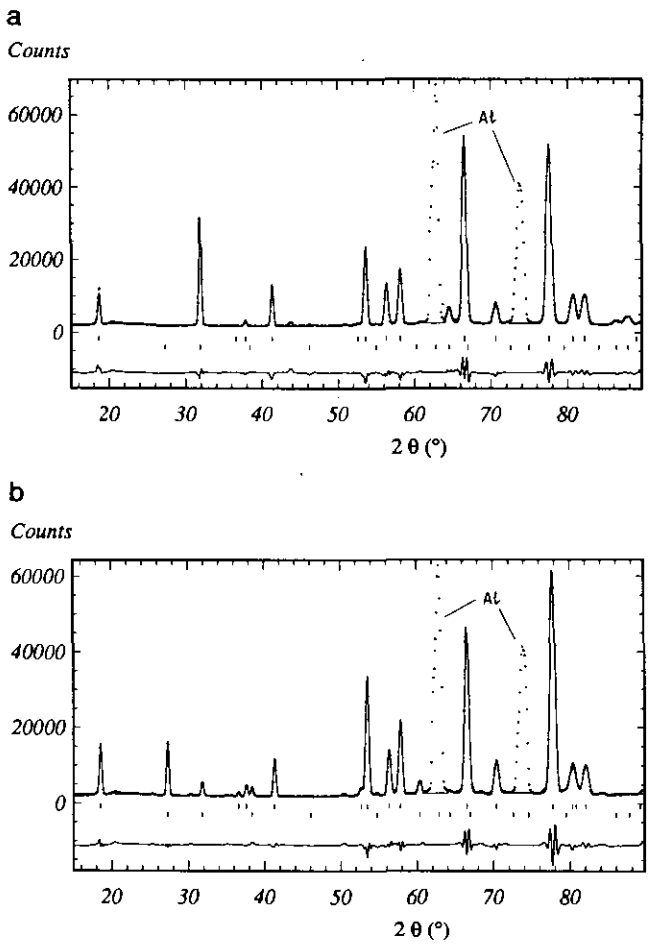

FIG. 5. Observed, calculated, and difference plots for compound (a) $YBa(Co_{1.6}Cu_{0.4})O_5$ at 1.4 K and compound (b) $YBa(Co_{1.1}Cu_{0.9})O_5$ at 1.4 K.

TABLE 4
Refined Structural Parameters of $YBa(Co_{2-x}Cu_x)O_5$ at 1.4 K

Atom	Position	x	y	z	Occupancy
Y	1(b)	0	0	0.5	1
Ba	1(a)	0.5	0	0	1
Cu/Co	2(h)		0.5	(A) 0.2678(8)	2
				(B) 0.2720(5)	
				(C) 0.2734(6)	
O_1	4(i)	0.5	0	(A) 0.3088(4)	4
				(B) 0.3128(3)	
				(C) 0.3130(4)	
O_2	1(d)	0.5	0.5	0	1

Note. A, $x = 0.4$; B, $x = 0.8$; C, $x = 0.9$; space group, $P4/mmm$.
Cell parameters:

	$a = b$ (Å)	c (Å)
A	3.8724	7.4953
B	3.8675	7.5238
C	3.8666	7.5266

TABLE 5
Distances in the (Cu, Co)O_5 Pyramid at 1.4 K

Composition x	(Co, Cu)–O_1 (Å)	(Co, Cu)–O_2 (Å)
0.9	1.956(1)	2.058(5)
0.8	1.958(1)	2.046(4)
0.4	1.961(1)	2.000(5)

corresponding to the domain ($0.3 \leq x \leq 0.75$) lie in the (001) plane. They are coupled antiferromagnetically within each $[(Cu, Co)O_2]_\infty$ layer, as well as along **c** (Fig. 6a). However, their direction in the (001) plane cannot be determined in our experiment, due to the tetragonal symmetry, and has been fixed arbitrarily along *a* axis.

Contrary to domain I, the Co(Cu) magnetic moments of domain II ($0.75 < x \leq 1$) do not lie in the (001) plane but exhibit another component along **c** (Fig. 6b). This explains the doubling of the *c* parameter for this second domain. In both domains I and II, the value of the magnetic moment $<\mu>$ increases as *x* decreases, i.e., as the cobalt content increases (Table 3).

The study of the magnetic structure of the $x = 0.8$ oxide versus temperature, in the range 1.4–380 K, allowed the R_M factors to be lowered to values ranging from 0.10 to 0.15 for the atomic coordinates listed in Table 6. The variation of the corresponding magnetic moments versus temperature (Fig. 7) clearly demonstrates that their spins switch up along the *c* axis as temperature approaches *T*2. One indeed observes that μ_x decreases to zero at *T*2.

Therefore temperature *T*2 characterizes the change of the orientation of the spins. In the range $T2 < T < T3$ the magnetic moments are all parallel to the *c* axis, as shown from the fit of the spectrum of the $x = 0.8$ sample registered at 380 K (Fig. 8).

TABLE 6
Atomic Coordinates of Cu, Co, and O_1 Sites at Different Temperatures of the $x = 0.8$ Composition

	T (K)				
	1.4	97	134	300	380
z(Cu/Co)	0.2720(5)	0.2722(5)	0.2726(5)	0.2736(5)	0.2735(11)
z_{01}	0.3128(3)	0.3131(3)	0.3131(3)	0.3136(3)	0.3144(7)

The evolution of the magnetic moments of the $x = 0.8$ oxide can be correlated to the geometry of the (Cu, Co)O_5 pyramids as shown from the interatomic distances (Table 7). One indeed observes that the equatorial Cu(Co)–O distances do not vary significantly as the temperature increases, whereas the Cu(Co)–O apical distance increases continuously. Such an evolution may be related to the alignment of the spins along **c** as the temperature increases. Thus it is most probably that a regular configuration of the Cu(Co)O_5 pyramid favors the inplane spin configuration, whereas the spin tends to switch along **c**, when the pyramid is elongated along the latter direction. This influence of pyramid elongation upon spin orientation can be produced either by the substitution of copper for cobalt at a fixed temperature or, for a given composition, by increasing the temperature. This interpretation is in agreement with the results obtained by Suard *et al.* (32) for the $YBa(Cu_{3-x}Co_x)O_7$ compounds, in which the spins are parallel to **c** for large (Cu, CO)–O apical distances (2.35–2.42 Å).

Taking into consideration the oxidation state of cobalt and copper determined by XANES, according to the formula $BaY(Co^{III}Co^{II}_{1-x}Cu^{II}_x)O_5$, the molar magnetic moments can be calculated and compared to the experimental deduced from neutron diffraction. For our calculation, the following usual magnetic moments of Cu(II), Co(II), and Co(III) in high-spin (hs), intermediate-spin (is), and

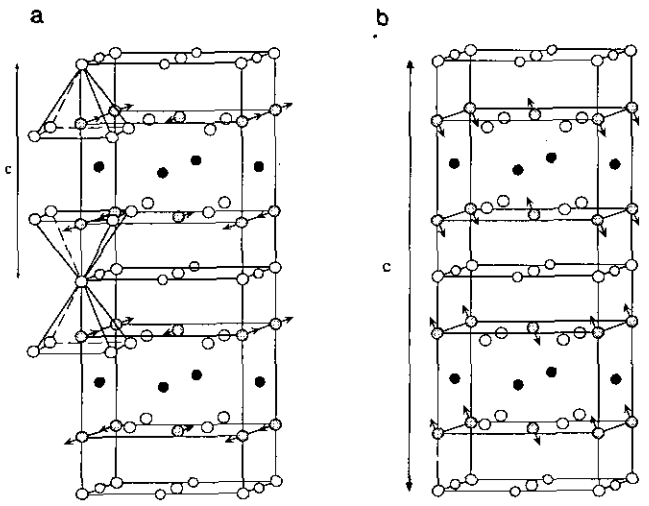

FIG. 6. Magnetic structures of $YBa(Co_{2-x}Cu_x)O_5$ compounds at 1.4 K. (a) Domain (I) $0.3 \leq x \leq 0.75$; (b) Domain (II) $0.75 < x < 1.0$.

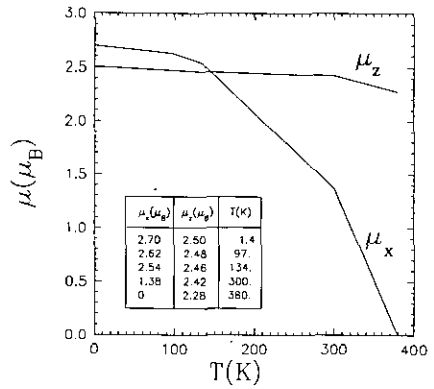

FIG. 7. Evolution of μ_x and μ_z vs temperature of YBa $(Co_{1.2}Cu_{0.8})O_5$ oxide.

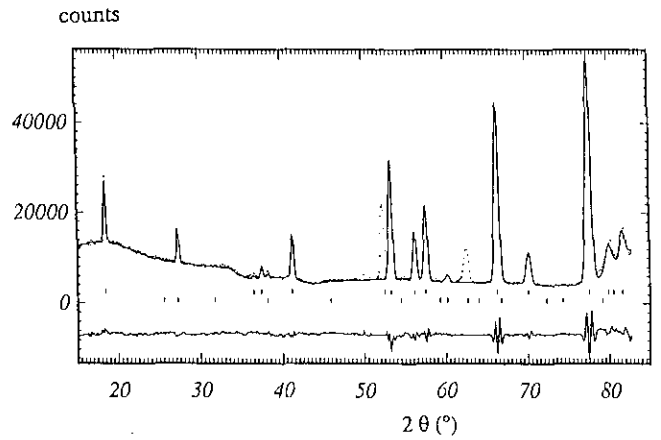

FIG. 8. Observed and calculated neutron profiles for YBa $(Co_{1.2}Cu_{0.8})O_5$ oxide at at 380 K.

low-spin state (ls) were used: $\mu_{Co_{hs}^{(II)}} = 3\ \mu_\beta$, $\mu_{Cu}^{(II)} = 1\ \mu_\beta$, $\mu_{Co_{hs}^{(III)}} = 4\ \mu_\beta$, $\mu_{Co_{ls}^{(III)}} = 2\ \mu_\beta$, $\mu_{Co_{ls}^{(III)}} = 0\ \mu_\beta$. The experimental values of magnetic moment at 1.4 K observed by neutron diffraction study and the different calculated values are given in Table 8. The good agreement between the experimental values and the calculated values corresponding to the intermediate spin shows that, in these phases, Co(III) ions have $t_{2g}^5 e_g^1$ configuration.

CONCLUSION

This study demonstrates the mixed valence of cobalt in the "112" structure, when copper remains divalent. It allows the spin configuration of Co(III) to be determined and shows that besides the antiferromagnetic to paramagnetic transition, a second transition occurs that is due to a change of the spin orientation of cobalt. Correlations between the spin orientation and the distortion of the (Cu, CO)O_5 pyramids are established for the first time.

A neutron diffraction study of the samples annealed in oxygen according to the formula $YBa(Co_{2-x}Cu_x)O_{5+\delta}$ will be performed in order to determine the influence of the excess oxygen on the magnetic structure of these phases.

TABLE 7
Interatomic Distances in the (Cu, Co)O_5 Pyramid at Different Temperatures of the $x = 0.8$ Compound

Temperature (K)	Cu/Co–O_1 (Å)	Cu/Co–O_2 (Å)
1.4	1.958(7) × 4	2.045(38) × 1
97	1.958(7) × 4	2.049(38) × 1
134	1.958(7) × 4	2.053(38) × 1
300	1.960(7) × 4	2.065(38) × 1
380	1.963(16) × 4	2.066(83) × 1

TABLE 8
Experimental and Calculated Molar Magnetic Moments at 1.4 K in the $YBa(Co_{2-x}Cu_x)O_5$ Compounds ($x = 0.9, 0.8, 0.4$)

Composition	μ^{exp} (μ_B)	μ^{cal} (μ_B) with $Co_{hs}^{(III)}$	μ^{exp} (μ_B) with $Co_{ls}^{(III)}$	μ^{exp} (μ_B) with $Co_{ls}^{(III)}$
$x = 0.9$	3.36	5.29	3.29	1.29
$x = 0.8$	3.68	5.48	3.48	1.48
$x = 0.4$	4.58	6.24	4.24	2.68

ACKNOWLEDGMENT

The authors thank P. Thuery for carrying out the neutron diffraction data.

REFERENCES

1. L. Er-rakho, C. Michel, Ph. Lacorre, and B. Raveau, *J. Solid State Chem.* **73,** 531 (1988).
2. R. A. Bari and J. Sivardiere, *Phys. Rev. B* **11,** 4466 (1972).
3. Z. Li-Ming, Thesis, Université de Bordeaux I, France, 1987.
4. R. A. Mohan Ram, K. K. Singh, W. H. Madhusudan, P. Ganguly, and C. N. R. Rao, *Mat. Res. Bull.* **18,** 703 (1983).
5. S. Ramaresha, T. V. Ramakrishnan, and C. N. R. Rao, *J. Phys. C. Solid State* **12,** 1307 (1979).
6. W. H. Madhusudan, K. Jagannathan, P. Ganguly, and C. N. R. Rao, *J. Chem. Soc. Dalton Trans.*, 1397 (1980).
7. B. Buftat, G. Demazeau, M. Pouchard, and P. Hagenmuller, *Mat. Res. Bull.* **18,** 1153 (1983).
8. J. C. Grenier, L. Fournes, M. Pouchard, and P. Hagenmuller, *Mat. Res. Bull* **21,** 441 (1986).
9. L. Barbey, N. Nguyen, V. Caignaert, M. Hervieu, and B. Raveau, *Mat. Res. Bull.* **27,** 295 (1992).
10. C. T. Lin, S. X. Li, W. Zhou, A. Mackenzie, and W. Y. Liang, *Physica C* **176,** 285 (1991).
11. J. Rodriguez, "Carvajal in Satellite Meeting on Powder Diffraction, Abstracts of the XVth Conference of the International Union of Crystallography," p. 127, Toulouse, 1990.
12. A. Bianconi, J. Budnick, A. M. Flank, A. Fontaine, P. Lagarde, A. Marcelli, H. Tolentino, B. Chamberland, G. Demazeau, C. Michel, and B. Raveau, *Phys. Lett. A* **127,** 285 (1988).
13. E. E. Alp, G. L. Goodman, L. Soderholm, H. B. Schuttler, S. M. Mini, M. Ramanathan, G. K. Shenoy, and A. S. Bommannavar, *J. Phys. Condens. Matter* **1,** 6463 (1989).
14. F. Baudelet, G. Collin, E. Dartyge, A. Fontaine, J. P. Kappler, G. Krill, J. P. Itie, J. Jegoudez, M. Maurer, Ph. Monod, A. Revcolevski, H. Tolentino, G. Tourillon, and M. Verdaguer, *Z. Phys. B* **69,** 141 (1988).
15. A. Bianconi, A. Clozza, A. Castellano, S. Dellalonga, M. De Santis, A. Dicicco, K. Garg, P. Delocv, A. Gargano, R. Giorgi, P. Lagarde, A. M. Flank, and A. Marcelli, *J. Phys. C* **9,** 1179 (1988).
16. T. Gourieux, G. Krill, M. Maurier, M. F. Ravet, A. Menny, H. Tolentino, and A. Fontaine, *Phys. Rev. B* **37,** 7516 (1988).
17. H. Tolentino, A. Fontaine, A. M. Flank, P. Lagarde, J. Y. Henry, J. Rossat-Mignod, T. Gourieux, G. Krill, and F. Studer, *Springer Ser. Solid State Sci.* **90** (1990).
18. B. Raveau, C. Michel, M. Hervieu, J. Provost, and F. Studer, *Springer Ser. Solid State Sci.* **90,** 66 (1990).
19. R. Retoux, F. Studer, C. Michel, B. Raveau, A. Fontaine, and E. Dartyge, *Phys. Rev. B* **41,** 193 (1990).

20. A. Bianconi, A. Congiu-Castellano, M. de Santis, P. Rudolf, P. Lagarde, A. M. Flank, and A. Marcelli, *Solid State Commun.* **63**(11), 1009 (1987).
21. A. Bianconi, A. Congiu-Castellano, M. de Santis, P. Delogu, A. Gargano, and R. Giorgi, *Solid State Commun.* **63**(12), 1135 (1987).
22. P. Kuiper, G. Kruizinga, J. Ghijsen, G. A. Sawatzky, and H. Verweij, *Phys. Rev. Lett.* **62**(2) 221 (1989).
23. A. Krol, C. S. Lin, Z. H. Ming, C. J. Sher, Y. H. Kao, C. T. Chen, F. Sette, Y. Ma, G. C. Smith, Y. Z. Zhu, and D. T. Shaw, *Phys. Rev. B* **42**(4), 2635 (1990).
24. A. Bianconi, M. De Santis, A. Di Cicco, A. M. Flank, A. Fontaine, P. Lagarde, H. Katayama-Yoshida, A. Kotani, and A. Marcelli, *Phys. Rev. B* **38**(10), 7196 (1988).
25. A. M. Flank, P. Lagarde, A. Bianconi, P. Castrucci, A. Fabrizi, M. Pompa, H. Katayama-Yoshida, and G. Calestani, *Phys. Scr.* **41,** 901 (1990).
26. F. Studer, N. Merrien, C. Martin, C. Michel, and B. Raveau, *Physica C* **178,** 324 (1991).
27. N. Merrien, F. Studer, A. Maignan, C. Martin, C. Michel, B. Raveau, and A. M. Flank, *J. Solid State Chem.* **101,** 237 (1992).
28. J. van Elp, "The Electronic Structure of Doped Late Transition Metal Monoxides," Ph.D. thesis, University of Groeningen, 1991.
29. M. Lenglet, R. Guillamet, J. Dürr, D.Gryffroy, and R. E. Vandenberghe, *Solid State Commun.* **74**(10), 1035 (1990).
30. N. Menyuk, K. Dwight, and P. M. Raccah, *J. Phys. Chem. Solids* **28,** 549 (1967).
31. V. Briois, C. Cartier, M. Momenteau, Ph. Maillard, J. Zarembovitch, E. Dartyge, A. Fontaine, G. Tourillon, P. Thiry, and M. Verdaguer, *J. Chim. Phys.* **86**(7/8), 1623 (1989).
32. E. Suard, V. Caignaert, A. Maignan, F. Bourée and B. Raveau, *Physica C* **210,** 164 (1993).